IEEE Access
Multidisciplinary | Rapid Review | Open Access Journal

Received August 22, 2019, accepted September 8, 2019, date of publication September 12, 2019,
date of current version September 27, 2019.

Digital Object Identifier 10.1109/ACCESS.2019.2940823

A Linearised Analysis for Structures With Synchronized Switch Damping

YAGUANG WU[1,2], LIN LI[1,2], YU FAN[1,2], JIUZHOU LIU[3], AND QIAN GAO[1,2]
[1]School of Energy and Power Engineering, Beihang University, Beijing 100191, China
[2]Beijing Key Laboratory of Aero-engine Structure and Strength, Beihang University, Beijing 100191, China
[3]China Academy of Launch Vehicle Technology, Beijing 100076, China

Corresponding author: Yu Fan (fanyu04@buaa.edu.cn)

This work was supported by the National Natural Science Foundation of China under Grant 11702011 and Grant 51675022.

ABSTRACT Synchronized Switch Damping (SSD) is a semi-active damping technology based on piezoelectric materials. It has advantages such as broadband and no need to tune. Despite the nonlinear governing equations, structures with SSD exhibit quasi-linear behaviour such as the resonant frequencies hardly vary with respect to energy level of excitation. Inspired by these phenomena, in this paper we propose a linearisation method for SSD, where the nonlinear force is equivalent to frequency-dependent viscous damping and linear stiffness coefficients. Closed-form expressions of these linearised parameters are given, making the method applicable both for lumped parameter models and finite element (FE) models. In the derivation a general force equation is used, so the linearised method is applicable for several typical variants of SSD, such as SSDS (S for 'on short-circuited'), SSDI (I for 'on inductance'), SSDV (V for 'on voltage') and SSDNC (NC for 'on negative capacitance'). The method is first validated against nonlinear simulations with harmonic and random vibration respectively, then further compared with experimental data in a published paper. Good agreements are found. We show that the proposed method can dramatically accelerate the computational efficiency, which is especially suitable for predicting the dynamic performance of complex structures with SSD. Eventually, a dummy integrally bladed disk with SSD is analysed to illustrate a potential application direction. There are more than 120k DOFs in the FE model, making full nonlinear simulation very time-consuming. However the simulation is finished within seconds by the proposed method and the typical damping characteristics of SSD are well captured.

INDEX TERMS Finite element model, integrally bladed disk, linearisation, nonlinear dynamics, synchronized switch damping, vibration reduction.

I. INTRODUCTION

Excessive structural vibration can lead to noise and mechanical failure, and further result in comfort and safety problems. Increasing damping is one of the major solutions to reduce vibration. Synchronized switch damping (SSD) proposed by Richard *et al.* [1], [2] is an promising candidate, for it is broadband, lightweight and stable. SSD basically consists in a switching circuit shunted to a piezoelectric patch which is embedded in or bonded to the host structure. The electrodes of piezoelectric materials are switched on/off at the voltage extrema of the piezoelectric patch in every vibration cycle. Consequently the voltage and the structural velocity are always in near opposite direction [3], providing a force that hinders vibration of the host structure.

The associate editor coordinating the review of this manuscript and approving it for publication was Luigi Biagiotti.

There are many other different choices of the shunting circuits to generate damping. For example one can shunt a circuit consists of resistors, inductors and capacitors to the electrodes, so that the vibration can be reduced by the electric dissipation and resonance [4]. However the performance of these passive circuits is either weak (resistor shunt [5]) or narrowband (inductor-resistor shunt [6]). To tune with multiple modes, the electric circuits may become rather complicated [7], [8] and the performance is essentially sensitive to modal frequencies. It has been well demonstrated that SSD has many advantages in comparison with the passive strategies [4], [9], [10]. SSD has improved multi-modal damping performance and it is insensitive with the variation of modal frequencies. For these reasons SSD based vibration control strategies are receiving increasingly research interests [3], [10]–[12] since it was proposed.

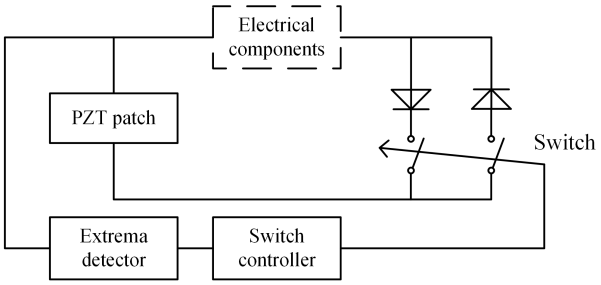

FIGURE 1. Schematic of SSD based circuit.

Several variants of SSD techniques have been defined, depending on the subsequent electric components. The first proposed one is synchronized switch damping on short circuit (SSDS) [1], where the switch is directly connected to the electrodes. A 1.3dB amplitude reduction is experimentally observed on a beam with SSDS [1]. In order to improve the damping effect, Richard *et al.* [2] put forward SSDI (SSD based on inductance). The idea is to connect an inductor in series with the switch, so as to magnify the voltage on the piezoelectric patch. The vibration reduction is 6dB for SSDI on the same beam. Lefeuvre *et al.* [13] proposed SSDV (SSD based on voltage source) by adding a pair of constant voltage sources with opposite polarity to the circuit. This also increases the voltage on the piezoelectric patch and thus enhance the damping. Badel *et al.* [11] found that the performance of SSDV is usually better than SSDI. The vibration reduction of SSDV even reaches 46dB experimentally for a cantilever beam. Qiu and Ji [14], Ji *et al.* [15] investigated SSDNC (SSD based on negative capacitance) where a negative capacitance is introduced into shunting circuit replacing the inductor. The damping performance of SSDNC depends on the value of negative capacitance which determines the voltage magnification.

The principal constitutions of SSD-based circuits include a piezoelectric patch bonded to the host structure, an extrema detection module, a switch control module and a switching circuit as illustrated by Figure 1. For a specific type of SSD, additional electric components are subsequently connected (e.g. inductor for SSDI). When the system is under excitation, the extrema detection module firstly identifies the maximum deformation of the system, then the switch control module generates a pulse signal to command the switch. The switch can be implemented by two electronic switches and diodes [16] or a pair of MOSFET transistors is alternative (shown by Figure 2) as declared by [2]. In terms of the extrema detector, it can either detect the maximum displacement of the system or the maximum voltage on the piezoelectric patch. The former is realized by obtaining displacement signal from eddy current sensor or displacement sensor [14]. The latter is achieved by acquiring directly the voltage signal on the piezoelectric patch [17], which is also called self-sensing [2]. The switch control module can be realised by a micro-controller board (Motorola MC6SHCI1) [2] or a DSP environment based on the dSPACE board DS1103 [16], [17].

Although a SSD circuit can be implemented in various ways, its essence is to achieve voltage reversal when the maximum displacement or voltage is detected in each vibration cycle. The closure of the switch is instantaneous and generally less than 1 ms, this time is very short compared with the vibrational period [1], the voltage applied on the piezoelectric patch can be expressed mathematically, which will be discussed in the following sections of the paper.

A large number of experimental studies have been carried out, however most of the host structures are beams [2], [13], [15], [17]. For implementations to complex structures (such as bladed disk in aero-engines), it is much more difficult to carry out experiments. There are also seldom numerical studies [18], [19], because nonlinear dynamic analyses are generally less efficient than the linear ones. The most commonly used numerical tool for steady-state response analysis is Multi-Harmonic Balance Method (MHBM) [20]. Although the efficiency is much higher than time-integral approaches, the computational cost increases significantly when the number of DOFs is relatively large (e.g. when a finite element model is used). In order to reduce calculating scale of the problem, Joannin *et al.* [21] developed the Component Nonlinear Complex Mode Synthesis method (CNCMS), and Liu *et al.* [19] applied it to design SSDNC dampers for bladed disks. In the process of CNCMS, nonlinear modes of each substructure need to be analyzed in advance [22]. Sometimes the selection of initial value will bring difficulties

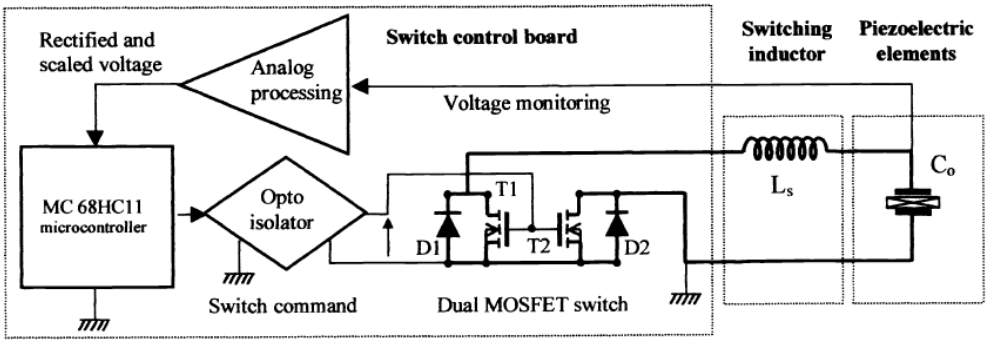

FIGURE 2. SSD circuits implemented by Richard *et al.* [2].

to convergence for models with large number of DOFs. For these reasons, currently most of the calculation for structures with SSD are based on lumped parameter models [1], [14], [18], [19]. Numerical tools for efficiently analyzing real-life engineering structures with SSD by FE models still require further development.

The application of SSD in vibration control of aerospace structures is promising (e.g. blisks) concerning its wide bandwidth and broad working range. However as mentioned above, the design process of the system with SSD using existed numerical approaches is time consuming because of its nonlinearity especially for large-scale models. Liu *et al.* [18] found that the nonlinear modal frequency and damping ratio of the system with SSD do not change with the vibration level. Inspired by the quasi-linear behaviour of SSD, we propose in the paper a new modelling method for the structure with SSD based on linearisation. In this method, the SSD is expressed analytically by a linear stiffness and a viscous damping, and both of them are independent to the vibrational amplitude.

Note that the proposed linearisation method is applicable to all kinds of SSD attached to any mechanical structures. Therefore, various kinds of SSD based on different structures are under investigation. In the following, we use a lumped parameter model with SSDNC and a beam finite element model with SSDS containing few DOFs to numerically verify the algorithm, respectively (Section III-C); to compare the results given by linearisation with published experimental data, a FE model of cantilever beam with a large number of DOFs is investigated (Section IV); the applicability to complex structures in industry and the high efficiency of the proposed method are further discussed by a blisk FE model with SSDNC (Section V).

II. REVIEW OF QUASI-LINEAR BEHAVIOUR OF SSD

Mathematically speaking, structures with SSD are nonlinear dynamic systems. But many of the observed characteristics are more consistent with linear systems. The most evident one is that the resonant frequencies of the system hardly vary with respect to the excitation level [18], [19], [23] and control parameters (inductance in SSDI [14] or negative capacitance in SSDNC [19]). These features are different from typical nonlinear systems (e.g. dry friction systems where resonant peaks shift under different normal force, or Duffing oscillators) so they are termed 'quasi-linear' in this paper. Detailed numerical and experimental results can be found in the aforementioned literature. In this section, we briefly introduce several typical SSD circuits and use a rather simplified model to review their quasi-linear behaviour. We also outline the numerical methods for nonlinear dynamic analysis used in this section.

A. MATHEMATICAL MODELLING OF SSD SYSTEMS

Here we use a 2-DOF lumped parameter model (shown by Figure 1) as an example. A piezoelectric spring is connecting masses m_1 and m_2, and a SSD circuit is shunted to the piezoelectric spring. No additional damping effects are taken into account. In this way such a structural system can only be damped by the SSD. The dynamic equations write as Eq. (1),

$$\begin{bmatrix} k_1+k_2+k_s & -k_2-k_s & a \\ -k_2-k_s & k_2+k_3+k_s & -a \\ a & -a & -C_p \end{bmatrix} \begin{Bmatrix} x_1 \\ x_2 \\ V \end{Bmatrix} + \begin{bmatrix} m_1 & & \\ & m_2 & \\ & & 0 \end{bmatrix} \begin{Bmatrix} \ddot{x}_1 \\ \ddot{x}_2 \\ \ddot{V} \end{Bmatrix} = \begin{Bmatrix} 0 \\ f_e \\ Q \end{Bmatrix} \quad (1)$$

where m_1 and m_2 refer to the mass, k_1 and k_2 refer to stiffness of the spring elements, a is the electromechanical coupling coefficient, k_s is the stiffness of the piezoelectric spring with short circuit, C_p is the capacitance of the piezoelectric spring, V is the voltage between the electrodes, Q is the electric quantity stored in the capacitance, and f_e is the excitation force.

Expanding the third equation in Eq. (1) at open circuit state (i.e. $Q = 0$), we obtain the following relationship:

$$V(t) = \frac{a}{C_p} u(t). \quad (2)$$

where $u = x_1 - x_2$ denotes the relative displacement. For system with SSD, the electrodes are open at most of the time, they are closed only when the displacement extrema is reached. We can therefore assume $V(t) = V_{SSD}(t)$, where $V_{SSD}(t)$ is the controlled voltage and in general it writes:

$$V_{SSD}(u, \dot{u}) = A_1 \max(u(t)) \text{sign}(\dot{u}(t)) + A_2 u(t) \quad (3)$$

where $\max(\bullet)$ denotes the maximizing with respect to time t, and $\text{sign}(\bullet)$ refers to the sign function. A_1 and A_2 are constants that depend on the type of SSD, namely:

$$A_1 = \begin{cases} \dfrac{a}{C_p}, & \text{SSDS} \\ \dfrac{(1+\gamma)a}{(1-\gamma)C_p}, & \text{SSDI} \\ \dfrac{a}{(1-\chi)C_p}, & \text{SSDNC} \\ \dfrac{(1+\sigma)(1+\gamma)a}{(1-\gamma)C_p}, & \text{SSDV} \end{cases}$$
$$A_2 = \frac{a}{C_p}, \quad \text{for all} \quad (4)$$

where coefficient γ refers to the voltage inversion factor for SSDI, χ denotes the capacitance ratio for SSDNC, and σ is the voltage ratio for SSDV. They can be directly derived from the governing equations and the details can be found in [16] and [18].

We can eliminate the voltage DOF by substituting Eq. (2) and Eq. (3) in Eq. (1), then Eq. (5) is obtained,

$$\begin{bmatrix} k_1+k_2+k_s & -k_2-k_s \\ -k_2-k_s & k_2+k_3+k_s \end{bmatrix} \begin{Bmatrix} x_1 \\ x_2 \end{Bmatrix} + \begin{bmatrix} m_1 & \\ & m_2 \end{bmatrix} \begin{Bmatrix} \ddot{x}_1 \\ \ddot{x}_2 \end{Bmatrix} + \begin{Bmatrix} f_{SSD} \\ -f_{SSD} \end{Bmatrix} = \begin{Bmatrix} 0 \\ f_e \end{Bmatrix} \quad (5)$$

where $f_{\mathrm{SSD}} = aV_{\mathrm{SSD}}$ is the nonlinear force generated by piezoelectric patch with SSD. The electromechanical coupling stiffness a is also called the voltage coefficient [15], which reflects the force generated by piezoelectric actuator under unit voltage as described by the aforementioned equation. Mathematically, the general form of the nonlinear force generated by SSD reads:

$$f_{\mathrm{SSD}}(u, \dot{u}) = aV_{\mathrm{SSD}} = B_1 \max(u(t))\mathrm{sign}(\dot{u}(t)) + B_2 u(t) \quad (6)$$

where $B_i = aA_i,\ i = 1, 2$ are constants depending on the type of SSD:

$$B_1 = \begin{cases} \dfrac{a^2}{C_{\mathrm{p}}}, & \text{SSDS} \\ \dfrac{(1+\gamma)a^2}{(1-\gamma)C_{\mathrm{p}}}, & \text{SSDI} \\ \dfrac{a^2}{(1-\chi)C_{\mathrm{p}}}, & \text{SSDNC} \\ \dfrac{(1+\sigma)(1+\gamma)a^2}{(1-\gamma)C_{\mathrm{p}}}, & \text{SSDV} \end{cases}$$

$$B_2 = \frac{a^2}{C_{\mathrm{p}}}, \quad \text{for all} \quad (7)$$

B. FORCED VIBRATION: MULTI-HARMONIC BALANCE METHOD

We can rewrite Eq. (5) in the matrix form:

$$\mathbf{M}\ddot{\mathbf{x}} + \mathbf{C}\dot{\mathbf{x}} + \mathbf{K}\mathbf{x} + \mathbf{f}_{\mathrm{SSD}} = \mathbf{f}_{\mathrm{e}} \quad (8)$$

where $\mathbf{K}$ is the stiffness matrix, $\mathbf{M}$ is the mass matrix, $\mathbf{C}$ is the structural damping matrix and in this section $\mathbf{C} = \mathbf{0}$, and $\mathbf{f}_{\mathrm{SSD}}$ referes to the nonlinear force generated by SSD. In practice the damping matrix can be determined by Rayleigh damping model, namely $\mathbf{C} = \alpha\mathbf{M} + \beta\mathbf{K}$ where α and β are constants. If a time-periodic external force is applied, e.g. $\mathbf{f}_{\mathrm{e}} \propto \sin(\omega t + \phi)$, a time-periodic response is anticipated when the influence of the initial conditions is damped. To calculate such steady-state response of the nonlinear systems, multi-harmonic balance method (MHBM) is widely used [20] for its high efficiency and numerical stability. The basic idea of MHBM is to transfer the unknown variables $\mathbf{x}$, the excitations $\mathbf{f}_{\mathrm{e}}$, and the nonlinear forces $\mathbf{f}_{\mathrm{SSD}}$ from time domain to frequency domain by Fourier analysis. Then the dynamic balance of forces can be expressed in terms of each harmonic term, and this shifts the ordinary nonlinear differential equations (8) into the algebraic nonlinear equations:

$$\tilde{\mathbf{H}}(\omega)\tilde{\mathbf{X}} + \tilde{\mathbf{F}}_{\mathrm{SSD}}(\tilde{\mathbf{X}}) = \tilde{\mathbf{F}}_{\mathrm{e}} \quad (9)$$

where $\tilde{\mathbf{X}}$, $\tilde{\mathbf{F}}_{\mathrm{SSD}}$, $\tilde{\mathbf{F}}_{\mathrm{e}}$ are the complex Fourier coefficients for $\mathbf{x}$, $\mathbf{f}_{\mathrm{SSD}}$ and $\mathbf{f}_{\mathrm{e}}$, respectively. Matrix $\tilde{\mathbf{H}}$ is the assembled dynamic stiffness matrix that consists of the dynamic stiffness matrix for each harmonic:

$$\tilde{\mathbf{H}} = \begin{bmatrix} \tilde{\mathbf{H}}_0 & & & \\ & \tilde{\mathbf{H}}_1 & & \\ & & \cdots & \\ & & & \tilde{\mathbf{H}}_{N_{\mathrm{h}}} \end{bmatrix}$$

where

$$\tilde{\mathbf{H}}_k = -(k\omega)^2\mathbf{M} + ik\omega\mathbf{C} + \mathbf{K}, \quad k = 0, 1, \ldots, N_{\mathrm{h}} \quad (10)$$

where $i = \sqrt{-1}$, N_{h} refers to the number of the truncated harmonics, and ω denotes the fundamental frequency which is equal to the excitation frequency. Note that the relationship between the frequency and the amplitude of the nonlinear force $\tilde{\mathbf{F}}_{\mathrm{SSD}}(\tilde{\mathbf{X}})$ is not (and probably cannot) explicitly expressed, the Alternating Frequency-Time (AFT) technique should be applied. In this way, we will first guess an initial value of $\tilde{\mathbf{X}}$ and solve Eq. (9) iteratively until a satisfying relative error is achieved. The convergence strongly depends on the choose of the initial value and the frequency step, and to improve numerical stability the arc-length continuation technique is recommended. For more details please refer to [24]. In addition, when the number of DOFs increases (e.g. FE models of complex structures), the analytical Jacobian matrix should be given instead of the numerical differential one in order to improve the convergence and accelerate the simulation [25]. Otherwise, the convergence failure might occur.

C. FREE VIBRATION: COMPLEX NONLINEAR MODAL ANALYSIS

For linear system, it is well known that the modal shapes and natural frequencies are independent to the external excitation or the level of the vibrational energy. This is no longer valid for nonlinear systems. As an extension of linear modes, a nonlinear mode is defined as: (1) a synchronized periodic motion named nonlinear normal mode (NNM) for conservative case [26] or (2) a synchronized decaying motion named complex nonlinear mode (CNM) for non-conservative case [27]. A nonlinear modal deformation is not necessarily time-harmonic [28], but we can use the superposition of several harmonics as an approximation:

$$\mathbf{x}(t) \approx \sum_{k=0}^{N_{\mathrm{h}}} \tilde{\mathbf{X}}_k e^{(-k\beta + ik\omega)t} \quad (11)$$

where ω is the fundamental frequency (also termed the nonlinear modal frequency), and β is the dissipative coefficient (also termed the nonlinear modal damping coefficient).

The MHBM can also be used to solve the CNM. By substitution Eq. (11) into Eq. (8) and ignoring the excitation term, the dynamic equations in frequency domain are derived:

$$\tilde{\mathbf{H}}(\beta, \omega)\tilde{\mathbf{X}} + \tilde{\mathbf{F}}_{\mathrm{SSD}}(\tilde{\mathbf{X}}) = \mathbf{0} \quad (12)$$

The dynamic stiffness for each harmonic becomes:

$$\tilde{\mathbf{H}}_k = (-k\beta + ik\omega)^2\mathbf{M} + (-k\beta + ik\omega)\mathbf{C} + \mathbf{K}, \quad k = 0, 1, \ldots, N_{\mathrm{h}} \quad (13)$$

Modal amplitude is defined as the norm of the first order fourrier coefficient for an arbitrary DOF [22] (e.g. the norm of $\tilde{\mathbf{X}}_{1,1}$ for the aforementioned case), which reflects the energy of the system. It has been recommended that to start the

TABLE 1. Parameters of the lumped parameter model.

Parameter	m_1	m_2	k_1	k_2	k_3
Meaning	mass 1	mass 2	spring 1 stiffness	spring 2 stiffness	spring 3 stiffness
Value	1kg	2kg	1.05N/m	0.35N/m	1N/m
Parameter	k_s	f_e	a	C_p	χ
Meaning	piezo spring stiffness	excitation force	voltage coefficient	piezo capacitance	capacitance ratio
Value	0.05N/m	0.001N	0.01N/V	1nF	0.5

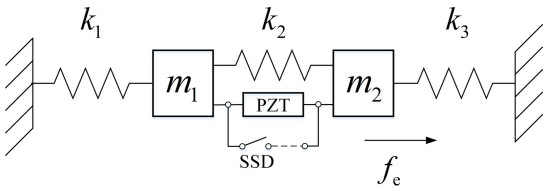

FIGURE 3. 2-DOF lumped parameter model with SSD.

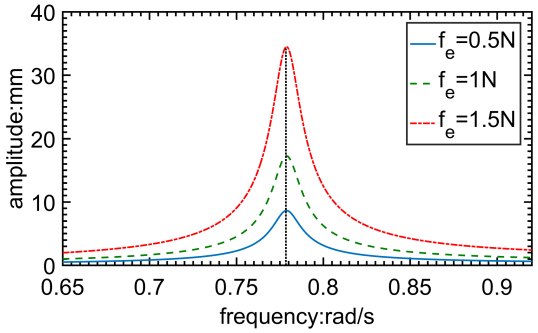

FIGURE 4. FRF of the system with SSDNC for different excitation amplitude around the first resonance for DOF 1.

computing from low energy level (or low modal amplitude), and to use a linear mode of the underlying linear system to initialize the nonlinear modal analysis [21]. By nonlinear modal analysis, the relationship between modal characteristic (i.e. modal frequency, damping ratio and modal shape) and modal amplitude can be generated.

D. QUASI-LINEAR BEHAVIOUR OF SSD

Using the aforementioned numerical tools, the forced response of the mass-spring model shown in Fig. 3 is calculated. Fig. 4 shows the frequency response function (FRF) of x_1 under different excitation level, and the SSDNC circuit with capacitance ratio $\chi = 0.5$ is considered. Full parameters are listed in Table 1. The quasi-linear behaviour of SSD is not model-dependant. For example, these features were also observed through a lumped parameter of blisk with SSDNC [23]. In this work, although a 2-DOF lumped parameter model with this set of parameters is used to illustrate the quasi-linear behaviour of SSD, certainly other models or parameters could be also chosen. In Table 1, the mass (m_1, m_2) and the stiffness (k_1, k_2, k_3) can be different for different mechanical structures. We can set them to other values if required. The capacitance ratio χ depends on the value of the negative capacitor connected in the circuit, and the range is (0, 1). The larger the ratio, the better the damping effect. However, if χ is close to one, the system might become unstable. Without loss of generality, we set $\chi = 0.5$. In [18], the quasi-linear behaviour was observed for $\chi = 0.5, 0.7, 0.95$. For piezoelectric patch available on the market (e.g. material: pzt5, size: 50mm×40mm×1.5mm), the intrinsic capacitance is around 1nf, hence we set $C_p = 1$nf for this model. The voltage coefficient a characterizes the conversion capability of mechanical energy and electrical energy. Generally, the value is small and can be measured experimentally. Basically the equivalent stiffness of the piezoelectric structure k_s should not significantly affect the nature frequency of the structure. Therefore k_s is smaller compared with the stiffness of the host structure. The choices of parameters of piezoelectirc patch such as k_s and a should respect the overall performance of the electromechanical coupling systems. That is, to ensure the modal electromechanical coupling factor (MEMCF) in the rational range (0.0001, 0.01). In this lumped parameter model, the MEMCF is 0.002. Therefore the parameters in Table 1 are reasonably set. If the parameters are set also in the rational parameter space but with different values, same phenomenon can be obtained.

In Fig. 4 the peak frequency does not deviate along with the excitation level, and this feature is different from typical nonlinear systems (e.g. dry friction or Duffing systems). The black dotted line connecting the resonance peaks is therefore a straight line. To illustrate this more clearly, we define the normalized response amplitude:

$$A_N = \frac{\omega^2 A}{f_0} \tag{14}$$

where A is the maximum response amplitude in the frequency band, and f_0 denotes the amplitude of the excitation. We can find in Fig. 5 that A_N does not change along with the excitation level. This indicates that the peak response varies in proportion with the excitation level, and the damping effect remains unchanged. This trend can be found for all the values of χ shown in Fig. 5.

The steady-state time-history of f_{SSD} force and relative displacement $(x_2 - x_1)$ are presented by the solid blue line and dotted orange line in Fig. 6 respectively, where the excitation amplitude is 1N. The force generated by SSDNC is indeed nonlinear with respect to the relative displacement. When the relative displacement reaches its maximum, the SSD force drops since the switch is closed. The SSD force hinders the movement at all times, which consequently provides damping. According to Eq. (6), when the sign of velocity $\dot{u}$ changes, the direction of nonlinear force generated by SSD reverses. Therefore f_{SSD} and velocity are in phase, and the phase lag between f_{SSD} and the displacement is almost $\pi/2$.

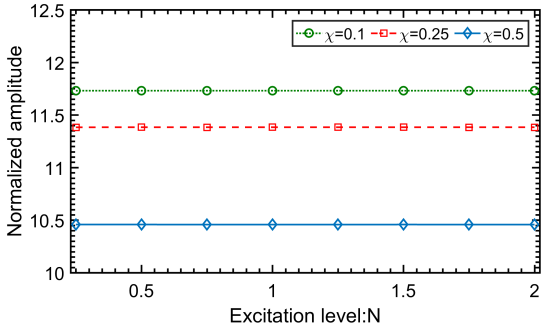

FIGURE 5. The maximum normalized frequency response amplitude under different excitation amplitude with different capacitance ratio.

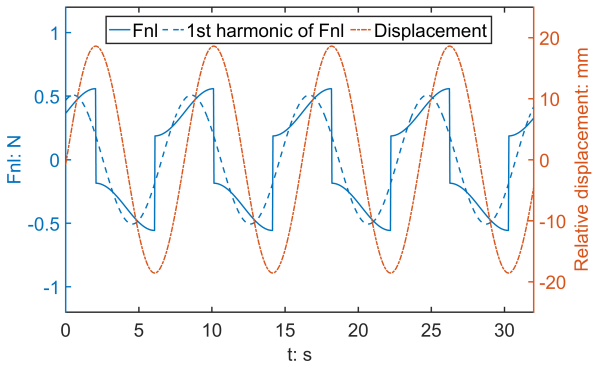

FIGURE 6. Nonlinear force generated by SSDNC, the first harmonic component of the nonlinear force by SSDNC and relative displacement in time domain under the excitation amplitude equals to 1N at 0.779 rad/s.

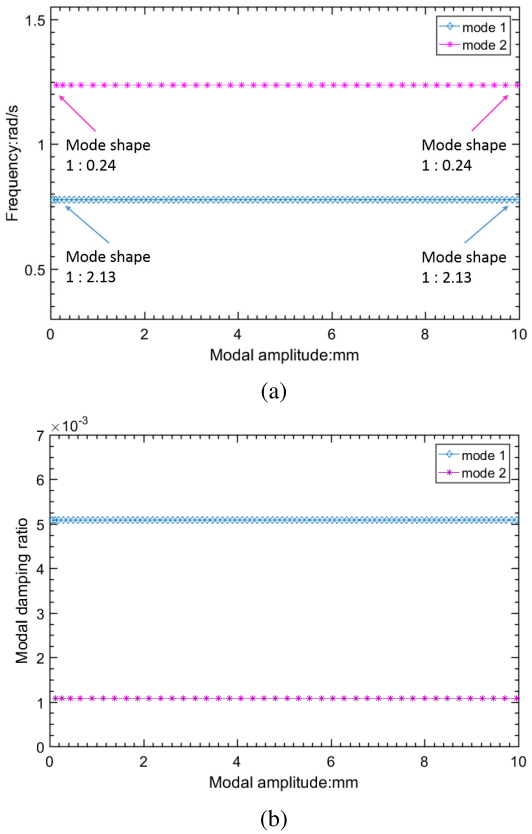

FIGURE 7. CNM for the 2-DOF lumped parameter model with SSDNC: (a) modal frequency and modal amplitude dependence (mode shape is described by the modal amplitude ratio of DOF1 and DOF2); (b) modal damping ratio and modal amplitude dependence.

This indicates that f_{SSD} is a damping force. In order to demonstrate the phase lag clearly, we extract the first-order harmonic of the nonlinear force through Fourrier analysis. As shown by the blue dotted line in Fig. 6, we can find that the first-order component is dominant. The phase lag between the orange line (i.e. displacement) and the blue dotted line (i.e. the first harmonic of the nonlinear force generated by SSD) can be easily observed.

The quasi-linear behaviour can also be shown through the nonlinear modal characteristics in Fig. 7. As mentioned, the nonlinear modal frequencies and shapes can vary with the modal amplitude in typical nonlinear systems. However for SSD systems, the nonlinear modal frequencies, shapes (Fig. 7a) and damping coefficients (Fig. 7b) remain nearly constant with respect to the modal amplitude. These results are consistent with that shown in Fig. 4 and 5. The backbone (black dotted line in Fig. 4) exactly matches the first modal branch in Fig. 7a.

The typical characteristics of nonlinear systems are: 1) The resonant peaks shift with respect to the excitation level [25]; 2) The response amplitude is not proportional to the excitation amplitude [29]; 3) Modal frequency and modal shape vary with energy level [30]; 4) Unstable solutions exist [31]. Taking the dry friction system as an example, if the excitation is sufficiently great, the dry friction system will perform like the underlying linear system without frictional damper [21], [32](i.e. the resonant frequency will be similar to that of the host structure, the damping ratio will tend to zero, and the vibrational amplitude will be very significant.) If the excitation is below certain value, the host structure and the damper will vibrate without relative displacement as an entity. The resonant frequency will be different from that under large excitation. Between these two extreme states, the damper will generate an optimal damping ratio at a certain excitation amplitude. For the Duffing systems, if the cubic stiffness coefficient exceeds a threshold, there will be three solutions at the same excitation frequency near the resonance. One of them is unstable, and the stability of the solutions needs to be determined by Floquet's theory [30].

However, these typical features are not significantly observed for systems with SSD. From both the forced response and the modal analyses (performed by Fig. 4, 5, and 7), we have observed that the overall dynamic behaviour of a structure with SSD dampers is very similar to a linear system (i.e. the frequency shift does not exist, the response is proportional to the excitation, and all solutions are stable) rather than a typical nonlinear one. Not limited to this simple model, quasi-linear behaviour can be observed by

nearly all structural systems with different kinds of SSD circuits, both in numerical analyses [18], [19], [23] and experiments [15], [33].

III. LINEARISED MODEL OF SSD

In this section, we will first give the derivation process based on the lumped parameter model, then extend to general finite element model. It is shown that both the equivalent viscous damping and stiffness coefficients can be given in closed-form. Numerical verifications are presented at the end of this section.

A. LINEARISATION ON SPRING-MASS MODELS

We recall that the nonlinear force generated by typical variants of SSD (SSDS, SSDI, SSDV and SSDNC) can be written in a unified mathematical form as shown in Eq. (6). There are two terms on the right side of Eq. (6), and the second one is the function of the displacement only. Therefore the equivalent stiffness can be directly written:

$$k_{\mathrm{eq}} = B_2 \tag{15}$$

The first term on the right side of Eq. (6) is the function of velocity only, which contributes to the damping. Here we assume that the relative velocity simply follows a sinusoidal function:

$$\dot{u} = V_0 \sin(\omega t + \phi) \tag{16}$$

where V_0 refers to the amplitude of the velocity. This is reasonable when the excitation is mono-frequency or in a relatively narrow frequency band, as presented in Fig. 6. We will further justify this assumption later in section III-C. In this way, the dissipative energy in one period can be expressed as the negative work done by the nonlinear force:

$$\begin{aligned} W_{\mathrm{SSD}} &= \int_{t=0}^{T} f_{\mathrm{SSD}}(t)\dot{u}(t)\mathrm{d}t \\ &= \int_{t=0}^{T} B_1 \max(u)\mathrm{sign}(\dot{u})\dot{u}\mathrm{d}t = \frac{4B_1 {V_0}^2}{\omega^2} \end{aligned} \tag{17}$$

where W_{SSD} refers to the dissipative energy per cycle by SSD. The dissipated energy of an linear viscous damper in one cycle is known as:

$$W_{\mathrm{eq}} = \int_{t=0}^{T} c_{\mathrm{eq}}\dot{u}\dot{u}\mathrm{d}t = \frac{c_{\mathrm{eq}} {V_0}^2 \pi}{\omega} \tag{18}$$

where W_{eq} is the equivalent dissipative energy by viscous damping, and c_{eq} refers to the equivalent viscous damping. Let $W_{\mathrm{SSD}} = W_{\mathrm{eq}}$, the damping coefficient can be found:

$$c_{\mathrm{eq}} = \frac{4B_1}{\omega\pi} \tag{19}$$

Thus, the SSD system is linearised, with equivalent stiffness k_{eq} shown in Eq. (15) and equivalent damping c_{eq} shown in Eq. (19). The nonlinear model shown in Figrue 3 is therefore transferred to a linear one as shown by Fig. 8. Note that the equivalent damping only depends on the frequency, and this explains the excitation independent feature observed

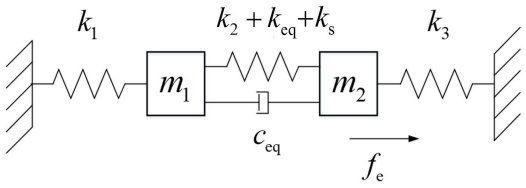

FIGURE 8. Equivalent linearisation model for lumped parameter model with SSD.

in section II-D. With these closed-form equivalent coefficients, the numerical simulation becomes much simpler comparing with MHBM or NCMS [19], [21], [34]. The linearised governing equations of Eq. (5) are expressed by Eq. (20).

$$\begin{aligned} &\begin{bmatrix} k_1 + k_2 + k_{\mathrm{eq}} + k_{\mathrm{s}} & -k_2 - k_{\mathrm{eq}} - k_{\mathrm{s}} \\ -k_2 - k_{\mathrm{eq}} - k_{\mathrm{s}} & k_2 + k_3 + k_{\mathrm{eq}} + k_{\mathrm{s}} \end{bmatrix} \begin{Bmatrix} x_1 \\ x_2 \end{Bmatrix} \\ &+ \begin{bmatrix} c_{\mathrm{eq}} & -c_{\mathrm{eq}} \\ -c_{\mathrm{eq}} & c_{\mathrm{eq}} \end{bmatrix} \begin{Bmatrix} \dot{x}_1 \\ \dot{x}_2 \end{Bmatrix} + \begin{bmatrix} m_1 & \\ & m_2 \end{bmatrix} \begin{Bmatrix} \ddot{x}_1 \\ \ddot{x}_2 \end{Bmatrix} = \begin{Bmatrix} 0 \\ f_{\mathrm{e}} \end{Bmatrix} \end{aligned} \tag{20}$$

B. LINEARISATION ON FE MODELS

Lumped parameter models are often obtained by parameter identification process, and parameters such as force coefficient of PZT patch need to be measured by experiments. Therefore, it is impossible to predict the dynamic performance of the real system through the lumped parameter model without experimental data. Even if the parameters are identified, the numerical simulation with lumped parameter model is not accurate because the high-order information of the model is neglected. Lumped parameter models are only effective for qualitative analysis.

On the contrary, FE models can be established according to the parameters of real structures, and the response of the system can be predicted quantitatively by numerical simulation before the experiment. Especially for the complex system which is not easy to implement the experiment prototype, numerical simulations based on FE models have great advantages.

Firstly, the nonlinear force generated by SSD in FE models is derived. Fig. 9 represents a general system bonded to N_{p} piezoelectric patches shunted by SSD circuits. For the sake of simplicity, only one piezoelectric patch shunted by SSD is considered in the formula derivation. The general equations of the piezoelectric mechanical coupling systems write as Eq. (21).

$$\begin{aligned} &\begin{bmatrix} M_{\mathrm{m}} & \\ & 0 \end{bmatrix} \begin{Bmatrix} \ddot{\mathbf{x}} \\ \ddot{U} \end{Bmatrix} + \begin{bmatrix} \mathbf{C}_{\mathrm{m}} & \\ & 0 \end{bmatrix} \begin{Bmatrix} \dot{\mathbf{x}} \\ \dot{U} \end{Bmatrix} \\ &+ \begin{bmatrix} \mathbf{K}_{\mathrm{m}} & \mathbf{K}_{\mathrm{mp}} \\ \mathbf{K}_{\mathrm{mp}}{}^{\mathrm{T}} & -C_{\mathrm{p}} \end{bmatrix} \begin{Bmatrix} \mathbf{x} \\ U \end{Bmatrix} = \begin{Bmatrix} \mathbf{f}_{\mathrm{e}} \\ Q \end{Bmatrix} \end{aligned} \tag{21}$$

There is only one electrical DOF (i.e. the voltage U) because the upper and lower surfaces of piezoelectric patch are electrodes, and the one of them is connected to ground. The matrix with subscript m refers to the matrix corresponding to mechanical DOFs, the subscript p denotes to the electrical DOF introduced by the piezoelectric patch. In Eq. (21),

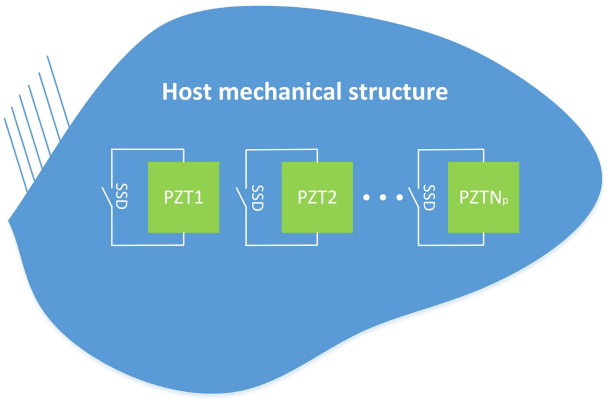

FIGURE 9. Schematic diagram of general mechanical structure bonded to piezoelectric patches shunted by SSD circuits.

C_p refers to the capacitance of the piezoelectric patch. $\mathbf{K}_{mp}$ denotes electromechanical coupling matrix.

For piezoelectric mechanical coupling systems with SSD, the voltage between the electrodes of piezoelectric patch is under control. Considering the first equation in matrix form of Eq. (21), the governing equations for SSD systems write:

$$\mathbf{M}_m\ddot{\mathbf{x}} + \mathbf{C}_m\dot{\mathbf{x}} + \mathbf{K}_m\mathbf{x} + \mathbf{f}_{SSD} = \mathbf{f}_e \tag{22}$$

where

$$\mathbf{f}_{SSD} = \mathbf{K}_{mp}U \tag{23}$$

refers to the nonlinear force generated by SSD applied to the mechanical system.

When the circuit is open, the current in the electrical circuit is zero. Hence the second equation of Eq. (21) becomes:

$$C_p{}^{-1}\mathbf{K}_{mp}{}^{T}\mathbf{x} = U_{op} \tag{24}$$

where U_{op} denotes the voltage at open circuit. Taking SSDS as an example, the controlled voltage applied to the piezoelectric patch could be expressed as:

$$\begin{aligned} U &= \max(U_{op})\mathrm{sign}(\dot{U}_{op}) + U_{op} \\ &= \max(\frac{\mathbf{K}_{mp}{}^{T}\mathbf{x}}{C_p})\mathrm{sign}(\frac{\mathbf{K}_{mp}{}^{T}\dot{\mathbf{x}}}{C_p}) + \frac{\mathbf{K}_{mp}{}^{T}\mathbf{x}}{C_p} \end{aligned} \tag{25}$$

Similar to the case of lumped parameter model, Eq. (25) indicates that when the voltage of the piezoelectric patch reaches its maximum, the piezoelectric patch will be short-circuited. Introducing Eq. (25) into Eq.(23), the nonlinear force generated by SSDS is then derived:

$$\begin{aligned} \mathbf{f}_{SSDS} &= \mathbf{K}_{mp}U \\ &= (\frac{1}{C_p}\mathbf{K}_{mp}\max(\mathbf{K}_{mp}{}^{T}\mathbf{x})\mathrm{sign}(\mathbf{K}_{mp}{}^{T}\dot{\mathbf{x}}) + \frac{\mathbf{K}_{mp}\mathbf{K}_{mp}{}^{T}\mathbf{x}}{C_p}) \end{aligned} \tag{26}$$

Using the same method as that of lumped parameter models, the negative work done by the nonlinear force for one period is:

$$\begin{aligned} W_{SSDS} &= \int_{t=0}^{T} \dot{\mathbf{x}}^{T}\mathbf{f}_{SSDS}dt \\ &= \frac{1}{C_p}\int_{t=0}^{T} \dot{\mathbf{x}}^{T}\mathbf{K}_{mp}\max(\mathbf{K}_{mp}{}^{T}\mathbf{x})\mathrm{sign}(\mathbf{K}_{mp}{}^{T}\dot{\mathbf{x}})dt \\ &= \frac{1}{C_p}\int_{t=0}^{T} \max(\mathbf{K}_{mp}{}^{T}\mathbf{x})|\mathbf{K}_{mp}{}^{T}\dot{\mathbf{x}}|dt \end{aligned} \tag{27}$$

For the structures with SSD, the force generated by SSD is applied only to the corresponding nodes attributed to piezoelectric patch. Considering the small proportion of piezoelectric material compared with the host structure, and the low inherent damping, the motion of nodes belonging to the piezoelectric patch could be regarded as synchronous. Under the assumption of the first order harmonic, the velocity of the mechanical DOFs is assumed as:

$$\dot{\mathbf{x}} = \mathbf{V}_0\sin(\omega t + \phi) \tag{28}$$

where $\mathbf{V}_0$ refers to the velocity amplitude vector of the mechanical DOFs. Introducing Eq. (28) into Eq. (27), the dissipative energy by SSDS for one period is then derived:

$$\begin{aligned} W_{SSDS} &= \frac{1}{C_p\omega}\int_{t=0}^{T} |\mathbf{K}_{mp}{}^{T}\mathbf{V}_0|^2|\sin(\omega t + \phi)|dt \\ &= \frac{4\mathbf{V}_0{}^{T}\mathbf{K}_{mp}\mathbf{K}_{mp}{}^{T}\mathbf{V}_0}{C_p\omega^2} \end{aligned} \tag{29}$$

If an equivalent viscous damping matrix is used, the equivalent dissipative energy in one cycle is derived:

$$W_{eq} = \int_{t=0}^{T} \dot{\mathbf{x}}^{T}\mathbf{C}_{eq}\dot{\mathbf{x}}dt = \frac{\mathbf{V}_0{}^{T}\mathbf{C}_{eq}\mathbf{V}_0\pi}{\omega} \tag{30}$$

Let $W_{SSDS} = W_{eq}$, the equivalent viscous damping matrix is:

$$\mathbf{C}_{eq} = \frac{4\mathbf{K}_{mp}\mathbf{K}_{mp}{}^{T}}{C_p\omega\pi} \tag{31}$$

The equivalent stiffness matrix is derived from the second term which is only the function of displacement vector on the right side of Eq. (26), the equivalent stiffness matrix writes:

$$\mathbf{K}_{eq} = \frac{\mathbf{K}_{mp}\mathbf{K}_{mp}{}^{T}}{C_p} \tag{32}$$

Since the forms of the nonlinear force generated by all types of SSD are similar mathematically, by employing the same derivation process, the equivalent viscous damping and stiffness matrix for FE models with SSD can be written

uniformly:

$$\mathbf{C}_{\mathrm{eq}} = \frac{4\mathbf{B}_1}{\omega\pi},\ \mathbf{B}_1 = \begin{cases} \dfrac{\mathbf{K}_{\mathrm{mp}}\mathbf{K}_{\mathrm{mp}}{}^{\mathrm{T}}}{C_{\mathrm{p}}}, & \text{SSDS} \\ \dfrac{(1+\gamma)\mathbf{K}_{\mathrm{mp}}\mathbf{K}_{\mathrm{mp}}{}^{\mathrm{T}}}{(1-\gamma)C_{\mathrm{p}}}, & \text{SSDI} \\ \dfrac{\mathbf{K}_{\mathrm{mp}}\mathbf{K}_{\mathrm{mp}}{}^{\mathrm{T}}}{(1-\chi)C_{\mathrm{p}}}, & \text{SSDNC} \\ \dfrac{(1+\gamma)(1+\sigma)\mathbf{K}_{\mathrm{mp}}\mathbf{K}_{\mathrm{mp}}{}^{\mathrm{T}}}{(1-\gamma)C_{\mathrm{p}}}, & \text{SSDV} \end{cases} \tag{33}$$

$$\mathbf{K}_{\mathrm{eq}} = \mathbf{B}_2, \quad \mathbf{B}_2 = \frac{\mathbf{K}_{\mathrm{mp}}\mathbf{K}_{\mathrm{mp}}{}^{\mathrm{T}}}{C_{\mathrm{p}}}, \quad \text{for all SSD} \tag{34}$$

Consistent to the conclusion of lumped parameter models, the equivalent damping matrix does not depend on the amplitude of the response. Therefore the damping generated by SSD for FE model is linear and can be replaced by the equivalent viscous damping matrix. The equivalent linearisation equations write:

$$\mathbf{M}_{\mathrm{m}}\ddot{\mathbf{x}} + (\mathbf{C}_{\mathrm{m}} + \mathbf{C}_{\mathrm{eq}})\dot{\mathbf{x}} + (\mathbf{K}_{\mathrm{m}} + \mathbf{K}_{\mathrm{eq}})\mathbf{x} = \mathbf{f}_{\mathrm{e}} \tag{35}$$

If the host structure contains multiple piezoelectric patches shunted with SSD, since each piezo patch is independent, the total equivalent damping or stiffness can be regarded as the sum of the equivalent damping or stiffness for each piezo patch shunted with SSD:

$$\mathbf{M}_{\mathrm{m}}\ddot{\mathbf{x}} + (\mathbf{C}_{\mathrm{m}} + \sum_{i=1}^{N_{\mathrm{p}}}\mathbf{C}_{\mathrm{eq},i})\dot{\mathbf{x}} + (\mathbf{K}_{\mathrm{m}} + \sum_{i=1}^{N_{\mathrm{p}}}\mathbf{K}_{\mathrm{eq},i})\mathbf{x} = \mathbf{f}_{\mathrm{e}} \tag{36}$$

where N_{p} is the number of the piezoelectric patches, $\mathbf{C}_{\mathrm{eq},i}$ and $\mathbf{K}_{\mathrm{eq},i}$ refer to the equivalent damping matrix and stiffness matrix by the i^{th} piezo patch with SSD, respectively.

If a model containing only two mechanical DOFs shunted by SSD is under investigation as shown by Fig. 3, then Eq. (22), Eq. (26) and Eq. (36) degenerate to Eq. (5) Eq. (6) and Eq. (20), respectively. Therefore, SSD linearisation theory based on lumped parameter models can be regarded as a special case of FE models.

As indicated by Eq. (33), the equivalent viscous damping of SSD is the function of the fundamental frequency of the excitation. The damping term is influential to the dynamic performance of the system in the resonant zone (i.e. the vibration frequency near resonance). Therefore, the limitation of the linearisation method is that the excitation spectra should only contain one resonant frequency of the structure. Otherwise, it brings the challenge to estimate the equivalent damping via Eq. (33). Further research dedicated to multi-frequency excitation is required.

C. NUMERICAL VERIFICATIONS

Applying the equivalent linearisation method firstly to the lumped parameter model with SSDNC introduced in Section II and comparing with the results by MHBM,

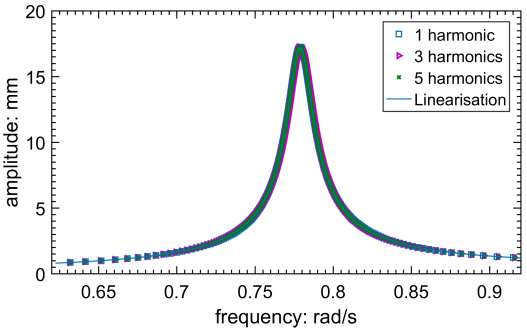

FIGURE 10. Comparison of FRFs by MHBM with different number of harmonics and the FRF by linearisation method based on 2-DOF lumped parameter model with SSDNC.

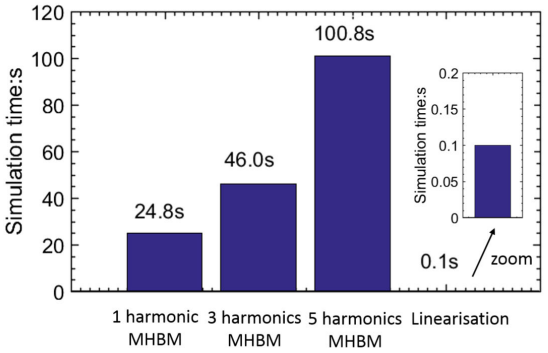

FIGURE 11. Comparison of simulation time for the 2-DOF lumped parameter model.

we obtain the FRFs as demonstrated by Fig. 10. It can be noticed that the number of harmonics retained has little effect on the results, keeping only the first order harmonic is sufficient to simulate the steady-state response accurately. The difference between the results by the proposed linearisation method and that by MHBM can be ignored. Therefore the correctness and accuracy of the proposed method is verified based on a representative lumped parameter model.

As far as concerned the efficiency, for MHBM with 1 harmonic, 3 harmonics and 5 harmonics, the simulation time are 24.8s, 46.0s and 100.8s. This is only for the 2-DOF model. With the augmentation of the number of DOFs, it can be predicted that the computing time will increase significantly. Even if only the first harmonic is retained, the calculation time will be very long. Whereas for the linearisation method, the simulation time is only 0.1s, the comparison of the cost time is performed by Fig. 11. The computational efficiency of the linearisation method has been dramatically increased comparing with the MHBM method.

For random excitation signals with a certain bandwidth, Newmark integral is adopted to predict the transient response of the 2-DOF model. The result by equivalent linearisation is compared with that by direct nonlinear analysis. The frequency band of the excitation contains 0.8 times to 1.2 times of the first-order resonant frequency (i.e. 0.779 rad/s), which is demonstrated by Figure 12a, the excitation signal in time domain is shown by Figure 12b.

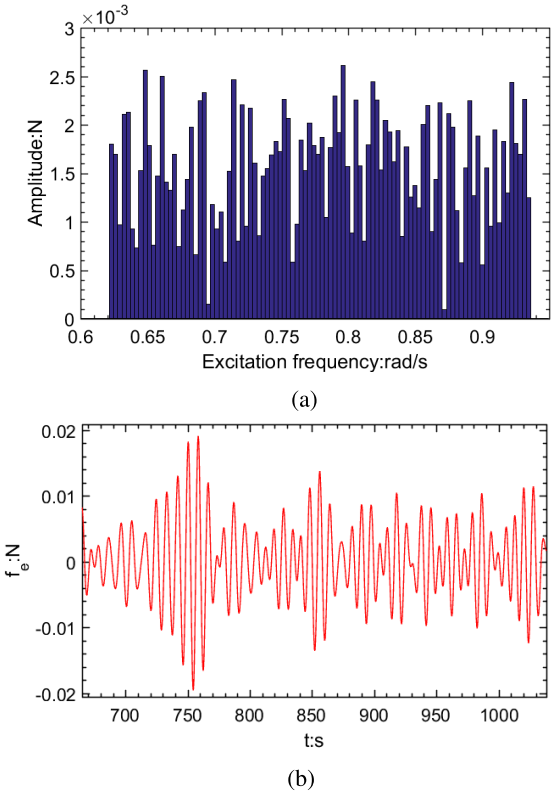

FIGURE 12. Random excitation with a certain bandwidth a. Signal in frequency domain. b. Signal in time domain.

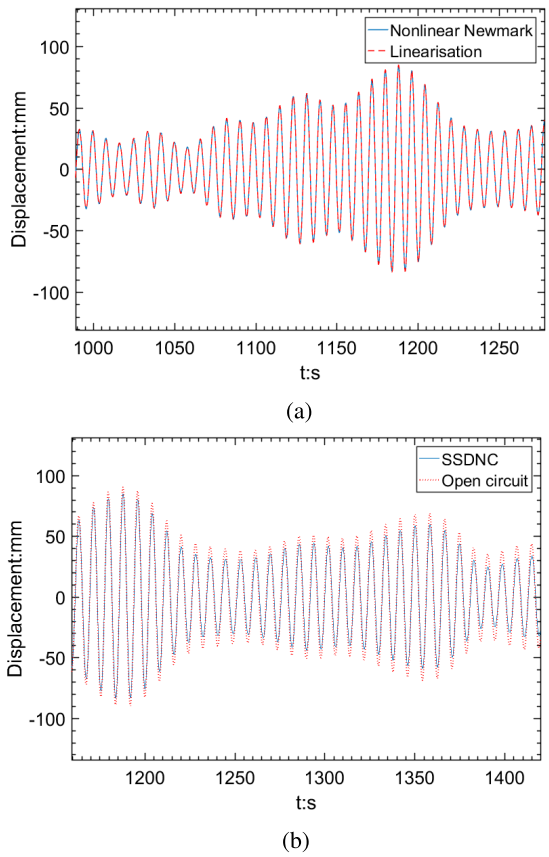

FIGURE 13. Time series of displacement under random excitation a. Comparison of direct nonlinear Newmark and linearisation method with SSDNC. b. Comparison of the system at open circuit state and with SSDNC.

Concerning the equivalent linearisation method under random excitation, due to the frequency dependence of the equivalent linearised damping as expressed by Eq. (19), and note that the frequency spectra of the random excitation contains not only one frequency component, therefore we estimate the equivalent damping by using the first resonant frequency. Fig. 13a performs the comparison of time series of the forced response by direct nonlinear analysis and equivalent linearisation. The results are basically consistent with relative error less than 3%. Fig. 13b shows the vibration reduction compared with the system at open circuit state, indicating that under random excitation, the vibration reduction effect of SSD is not as good as that under harmonic excitation. We can conclude that the equivalent linearisation method has high accuracy under random excitation with the band only containing one resonance.

Through the above analyses, we can conclude that the linearisation method of SSD can capture both the steady-state performance and the transient response under random excitation for lumped parameter models with SSD. The results are numerically verified by MHBM and Newmark integral respectively. The efficiency of the proposed method is much higher than traditional nonlinear solvers.

Next we will use a FE model to further verify the proposed method. In this case, results calculated by MHBM will be regarded as baseline. Since the algorithm of MHBM is also coded by the authors, the Newmark method will be adopted to validate the program.

A simple cantilever beam model attached by a PZT patch with coarse mesh is under investigation (shown by Fig. 14a), the voltage DOFs on the upper electrode of PZT patch are coupled. On the lower electrode, the voltage is set to zero. There are totally 45 nodes (except for the clamped nodes) containing 136 DOFs (including one electrical DOF). Only mechanical DOFs belonging to the PZT patch are under nonlinear force, thus the number of nonlinear DOFs is 45.

To verify the linearisation method for the FE model, both the MHBM method and Newmark method are used to calculate the steady-state response. The maximum displacement of the node in one period at steady-state is recorded as the response amplitude at the excitation frequency.

The target mode is set as the first bending mode as instance. The modal frequency is 586.7Hz at open-circuit state, and the modal shape is presented by Fig. 14b.

Fig. 15. compares the results calculated by the proposed linearisation method, the MHBM and the Newmark for the cantilever model with SSDS. Good agreements can be found. At each calculated frequency point, the relative error is less than 2%, which is acceptable. A filtering process of velocity in time domain is indispensable for Newmark method due to the symbolic function in the expression of nonlinear force generated by SSD. The error might be caused by the low

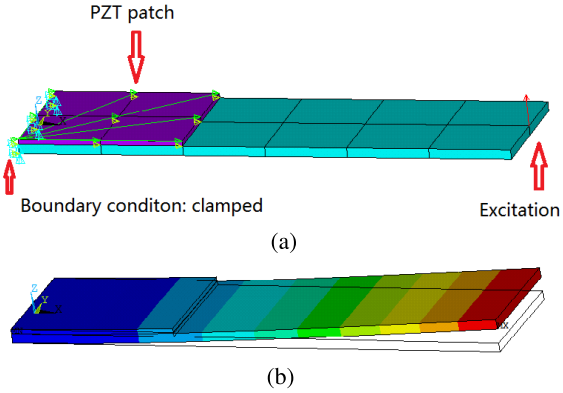

FIGURE 14. a. FE model of a cantilever beam attached by a PZT patch with coarse mesh. b. The first bending mode at open-circuit state.

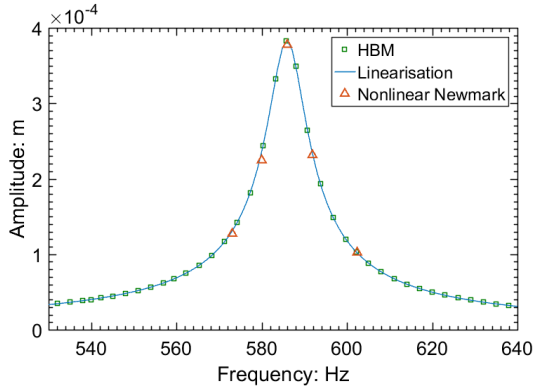

FIGURE 15. Comparison of results by linearisation method and nonlinear methods (MHBM and Newmark) for the cantilever beam FE model with SSDS.

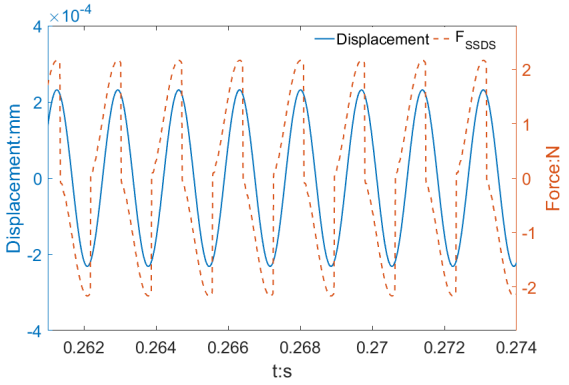

FIGURE 16. Sequential displacement and nonlinear force generated by SSDS calculated by Newmark integral at 580.1 Hz.

pass filtering. Fig. 16. performs the displacement and nonlinear force generated by SSDS in time domain calculated by Newmark integral at 580.1 Hz.

Table 2 lists the simulation time for the three numerical methods. It can be seen that the Newmark integral requires a long calculation time in order to obtain the steady-state at each frequency. The efficiency of harmonic balance has been improved compared with the Newmark method. The proposed linearisation method reduces the calculation time

TABLE 2. Comparison of simulation time for the coarse FE model of cantilever beam with SSDS.

Model information:	Beam	Total DOFs 136	Nonlinear DOFs 45
Methods	Newmark	MHBM	Linearisation
Total time cost	108.25s	11.62s	0.08s
Time per frequency	12.65s	0.29s	0.0007s
Relative Error	1.8%	0%	1.1%

to trace a FRF curve to 0.7% compared with the harmonic balance one even though the frequency resolution is much higher.

IV. COMPARISON WITH PUBLISHED EXPERIMENTAL DATA

In order to further verify the proposed equivalent linearisation method, we use the experimental data from an already published paper by Ji *et al.* [14] in terms of single mode control for SSDI. This experiment is conducted on a cantilever beam attached by two PZT patches on the top and the bottom surface of the beam. For the finite element modeling of the experimental beam, in order to make the calculation independent to the mesh density, the number of DOFs has been significantly augmented compared with the case in Section III-C. In order to further explain the correctness and efficiency of the linearisation algorithm on large-scale model, the widely-used harmonic balance method is also taken as a comparison. Since the MHBM has been already verified by Newmark integral in Section III-C, and the computational cost of Newmark could be enormous in terms of large-scale models, Newmark will be no longer employed.

The configuration of the composite beam used in the experiment is shown by Fig. 17a. The beam is clamped on an electromagnetic shaker for excitation which generates harmonic excitation. The distance between left edge of the piezoelectric elements and the clamped end of the beam is 10 mm as shown in Fig. 17b. The vibrational level of the beam is quantified by the vertical displacement amplitude at a distance of 290 mm from its clamped end. The parameters of the beam and the PZT patches used in this experiment are listed in Table 3 and Table 4 respectively, which are used for numerical simulations later.

The FE model is established in Ansys at open circuit shown by Fig. 17b. The beam is modeled by SHELL 181 element, and the PZT patches are modeled by SOLID 5. The number of DOFs is 16199 so that the simulation result is independent to the mesh. Fig. 18a. and 18b. illustrate the 1st modal shape (1st bending) and the 2nd modal shape (2nd bending) of the cantilever beam attached by a piezo-patch at open circuit, respectively. The 1st modal frequency is 10.4Hz, and the 2nd modal frequency is 62.2Hz.

With the value of the resistance and the impedance in the shunting circuit, the voltage inversion factor γ can be derived [18], which is equal to 0.58 for the system with SSDI. The equivalent damping and stiffness generated by SSD can then be calculated. By using the structural matrix and the calculated equivalent matrix, the linearisation method can be

TABLE 3. Parameters of the cantilever beam.

Variable	Length (mm)	Width (mm)	Thickness (mm)	Elastic modulus E1 (Gpa)	Elastic modulus E2 (Gpa)	Poisson ratio	Shear modulus (Gpa)	Density (kg/m3)
Value	300	50	1.2	16.5	35.2	0.109	12.5	1900

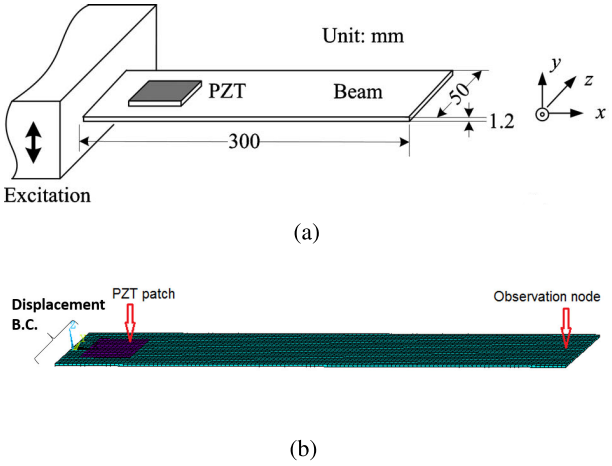

FIGURE 17. a. Configuration of the experimental system (Ji *et al.* JVA, 2011); b. Finite element model of the experiment system.

TABLE 4. Parameters of the piezoelectric patches.

Material	Length (mm)	Width (mm)	Thickness (mm)	Elastic modulus (Gpa)	Poisson ratio
PZT	30	30	0.2	59	0.345

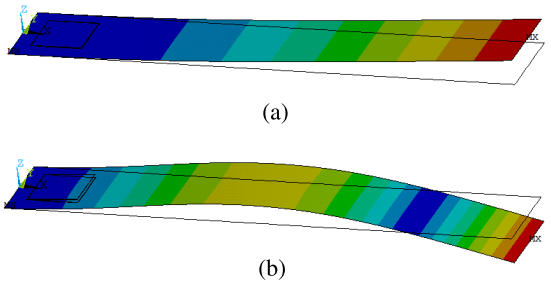

FIGURE 18. Modal shape of the cantilever beam with PZT patch at open circuit state: a. 1st bending mode; b. 2nd bending mode.

executed in Matlab. It is noteworthy that unlike the lumped parameter model, all the parameters of the experimental sample are taken directly in the numerical simulation process. This will improve the accuracy of simulation. The parameters of the numerical model, especially those of piezoelectric materials, are calibrated with the open circuit experimental data of the first resonance (i.e. resonant frequency and amplitude), because the parameters of PZT materials given by the experiment are not sufficient in terms of modelling. The calibrated data of PZT materials are listed in Appendix.

Firstly the simulation result by linearisation is compared with the result calculated by harmonic balance method. Good agreements are confirmed at the frequency range where the two resonance peaks belong to as performed by Fig. 19, and the relative error is less than 5%. The result by HBM

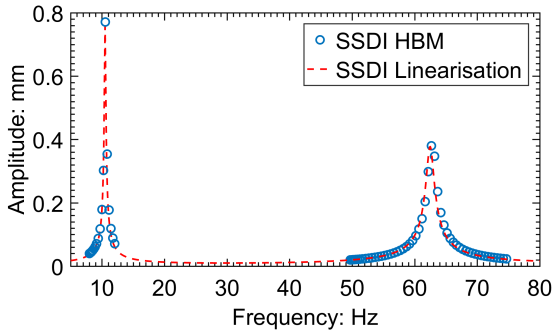

FIGURE 19. Comparison of FRFs by linearisation and HBM based on the finite element model of the cantilever beam with SSDI.

TABLE 5. Comparison of harmonic balance method and linearisation method for large-scale FE model of cantilever beam with SSDI.

Model information: experimental beam	Total DOFs 16199	Nonlinear DOFs 1027
Methods	HBM	Linearisation
Total time cost	2965.86s	160.22s
Time per frequency	40.08s	0.29s
Relative Error	0%	<5%

is just calculated around the resonances where the damping is sensitive to the dynamic performance in order to avoid computational burden. The simulation time for these two methods are listed in Table 5. We notice that the efficiency of linearisation is much higher than HBM for large-scale model. The time cost of linearisation is 5% of HBM.

Secondly, the simulation resuls by linearisation are compared with the published experimental data. The FRFs by linearisation are plotted in Fig. 20. The comparison of the results from numerical simulation and by experiment is summarized in Table 6. The relative error for resonant frequency is 1% for the 1st mode and 8.6% for the 2nd mode. For the resonant amplitude, the errors are less than 12.5% for these two modes. The attenuation of the 1st resonant amplitude is −4.3dB from experiment and −4.7dB by numerical simulation compared to the open state. For the 2nd resonant peak, the attenuation is −2.3dB and −3.8dB for experiment and simulation, respectively. We notice that the damping effect of numerical simulation is better than that of experiment, because the turning time of the switch in simulation is neglected, which avoids the loss of work done by the force generated by SSDI.

The error might be caused by the boundary conditions and the inaccurate material parameters especially for PZT patches, since the piezoelectric parameters provided by the experiment are not complete to modeling numerically. This is also the reason why the case with SSDNC in [14] is not under investigation in this paper, the intrinsic capacitance of the

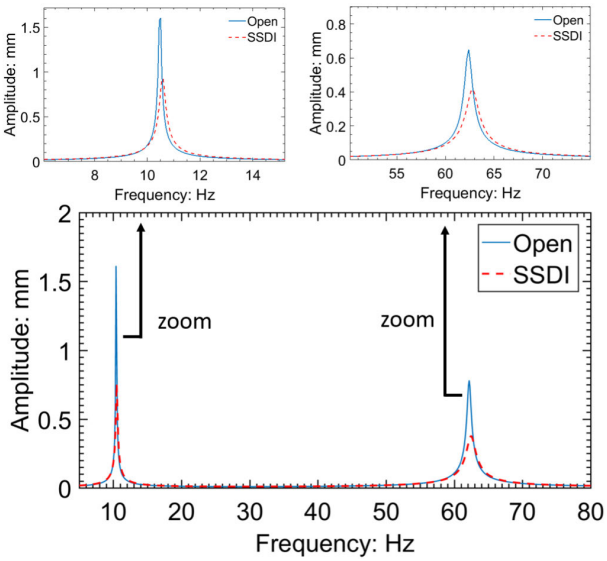

FIGURE 20. FRFs for the shunting system at open circuit state and with SSDI by linearisation numerical simulation.

TABLE 6. Summarization of results by linearisation method and by experiment.

	Experiment	Simulation	Error
1st resonant frequency (Hz)	10.4	10.5	1.0%
1st resonant amplitude at open state (mm)	1.59	1.60	1.3%
1st resonant amplitude with SSDI (mm)	0.96	0.93	2.9%
2nd resonant frequency (Hz)	68.8	62.9	8.6%
2nd resonant amplitude at open state (mm)	0.65	0.65	0.0%
2nd resonant amplitude with SSDI (mm)	0.48	0.42	12.5%

piezoelectric patch generated by FE model is quite different from that measured in experiment.

Even though the numerical results are slightly different from the experiment, the numerical results are sufficient to predict the dynamic performance of the system with acceptable accuracy. For FE models with a great number of DOFs the efficiency is sufficiently high (e.g. considering this case, the simulation time is about 160s for each FRF curve).

V. APPLICATION: VIBRATION CONTROL OF BLADED DISKS BY SSD

Bladed disk is the assembly of the disk and the mounted blades in aeroengines. When the aeroengine operates in the rotating state, the bladed disk of compressor works on the gas, or the gas works on the bladed disk of turbine. The interaction between the rotating bladed disk and the complex flow field makes it suffers severe aerodynamic load. Since the bladed disk rotates in the flow field, from an observing point fixed on the blisk, the excitation generated by the flow field and applied to the blisk can be regarded as rotational load, which is composed by circumferential travelling waves with different engine order (EO). The EO describes the number of harmonic waves along circumferential direction It also reflects the phase difference between the excitation force at each sector. Due to the high modal density of bladed disks, it is difficult to avoid all the resonances in the design process. Therefore, bladed disks often experience high vibration

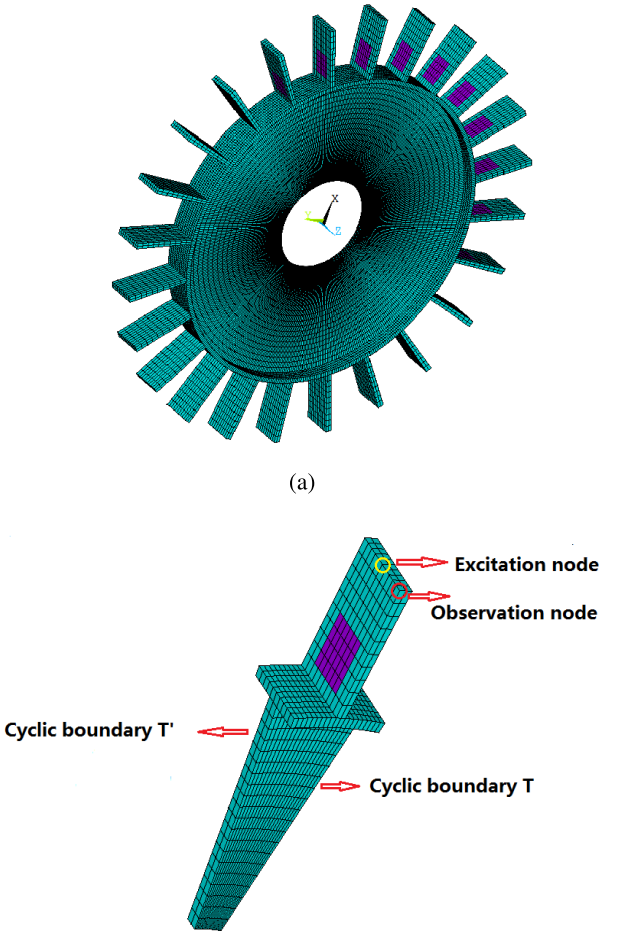

FIGURE 21. a. FE model of the blisk; b. FE model for the expanded sector.

levels, leading to high cycle fatigue (HCF) which might cause structural failure. Frictional damping is a traditional way to reduce the vibration level of bladed disks. Joints or contact interfaces in bladed disk assemblies can bring frictional damping. Relative displacements at these frictional interfaces generate energy dissipation thus the vibration level decreases [29], [34], [35]. In recent years, in order to improve aerodynamic performance and reliability, the integral bladed disk (blisk) as single-piece-made component is developed and implemented industrially [36]. However, due to the lack of joints and connections where energy dissipation by friction could occur, the damping decreases dramatically and vibration problem becomes more prominent. For these reasons, it is necessary to investigate new damping strategies for blisks.

Piezoelectric damping is a developing damping technology [4] since 1990s. More and more scholars try to control the vibration of blisk via piezoelectric damping technologies [23], [37]–[39], including passive piezoelectric shunted damping, piezoelectric network and SSD. Considering the advantages of semi-active piezoelectric damping technology based on SSD, such as multi-modal damping effect and insensitivity to working conditions, it seems that the SSD provides

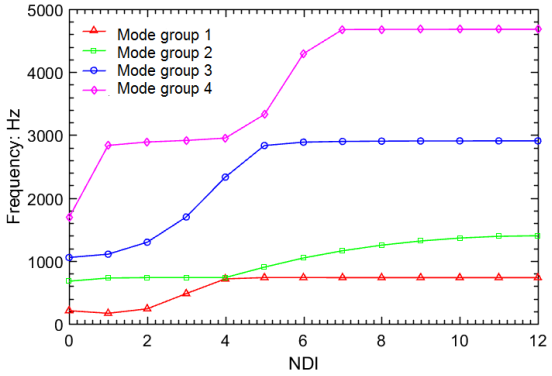

FIGURE 22. Modal frequencyâĂ" nodal diameter index (NDI) diagram of the blisk model embedded with PZT patch at short circuit state (only 1-4 modal groups are demonstrated).

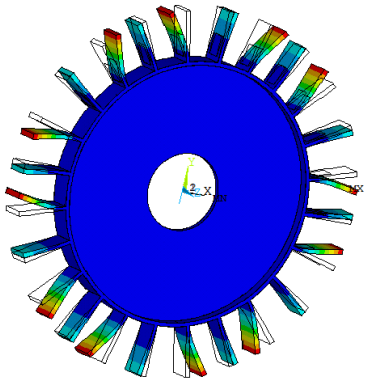

FIGURE 23. Modal shape for the blisk with SSD at short circuit state: mode (NDI 6, 1st mode group).

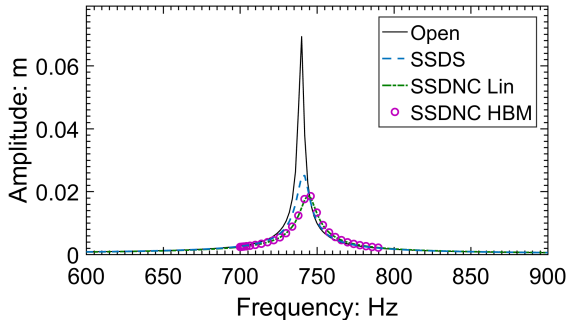

FIGURE 24. The comparison of FRFs of the blisk embedded with PZT patches at open circuit state, shunted by SSDS and SSDNC for the mode (NDI 6, 1st group).

the prospect of application for blisks. For the studies of blisks with SSD, according to the authors' knowledge, no experiments have been implemented. Due to the complexity of the structure, numerical simulation is a feasible way of investigation for blisks with SSD [18], [19]. For numerical studies, lumped parameter models were used, and the steady-state response of the system was calculated by nonlinear solver either by MHBM [18] or CNCMS [19]. Comparing with Newmark integral, the computational efficiency has been improved, but with the increase of DOFs, the computational burden will be still heavy, and even the risk of convergence failure will arise. This might be the reason why research concerning about blisks with SSD were often based on lumped parameter models. In order to quantitatively study the effect of SSD on blisks vibration reduction, generally FE models should be applied, leading to a great number of DOFs. It is time-consuming to employ nonlinear algorithm such as Newmark integral or MHBM especially for parameter analysis. Therefore, the proposed linearisation method is especially suitable for the design of blisks with SSD.

In this section, a dummy blisk FE model with SSD shunted in each sector is under investigation by the proposed linearisation method. Although this model is not from a real blisk, on the one hand, it is sufficient to describe typical nodal-diameter vibration of blisk, on the other hand, it has enough DOFs. Therefore this dummy blisk model can be used to verify the potential industrial implementation in the design process of blisks with SSD by the linearisation method. Thanks to the cyclic periodicity of the blisk, cyclic reduction technique can be used by projecting physical coordinates to traveling wave space, thus the number of DOFs is reduced to the dimension of a sector.

Fig. 21a demonstrates the FE model of the blisk, PZT patches (purple) are embedded on blades. There are 24 sectors. For this case, only the FE model of the expanded sector needs to be established (shown by Fig. 21b). The DOF number of the sector is 5968. The engine order excitation is applied on the excitation node marked in Fig. 21b. The direction of the exciting force is perpendicular to the blade, and the amplitude is 100N. Another node marked as observation node is used to display the response. The maximum displacement of the observation node is regarded as an index to quantify the vibrational level. In this study, the Craig-Bampton (CB) modal reduction technique is also implemented to decrease the further calculating scale. The DOFs belong to PZT patch, the excitation DOF, the cyclic boundary DOFs, and the DOFs belong to observation node should be kept in physical coordinates in the CB reduction process. Other linear DOFs are replaced by modal coordinates. After the CB reduction, the retained number of DOFs is 463.

Blisks normally exhibit vibration with different nodal-diameters, and nodes on nodal-diameters do not vibrate. This nodal-diameter phenomenon is the modal characteristic of blisks, which is described by frequency - nodal diameter index (NDI) diagram. The modal frequency - NDI diagram of the blisk model embedded with PZT patch at short circuit state is illustrated in Fig. 22. Only the first four modal groups are plotted. The modes at the horizontal position of modal group lines are dominated by blade, whereas the modes at slope position are disk dominated. The modes in frequency steering zone (i.e. the nearest zone between two consecutive groups) are coupling mode, indicating that both blade and disk vibrates.

Fig. 23 shows the modal shape of the blisk with embedded PZT patches at short circuit state. The NDI of the mode is 6, and it belongs to the 1st modal group. This mode is blade dominated. It can be observed from Fig. 24 that compared

TABLE 7. Vibration Reduction of different SSD technologies for different modes.

	Type	Response peak for SSDS Compared to open circuit	Response peak for SSDNC Compared to open circuit
Mode (NDI 6, 1st group)	Blade dominated (bending)	-59%	-73%
Mode (NDI 8, 4th group)	Blade dominated (higher order bending)	-41%	-55%
Mode (NDI 6, 4th group)	Coupling (blade torsion)	-47%	-62%

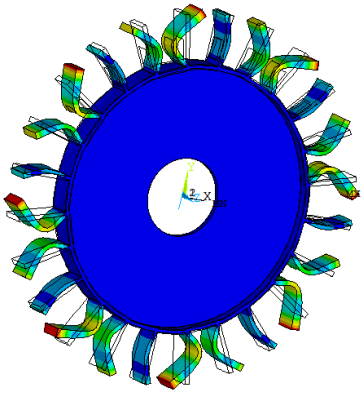

FIGURE 25. Modal shape for the blisk with SSD at short circuit state: mode (NDI 8, 4th modal group).

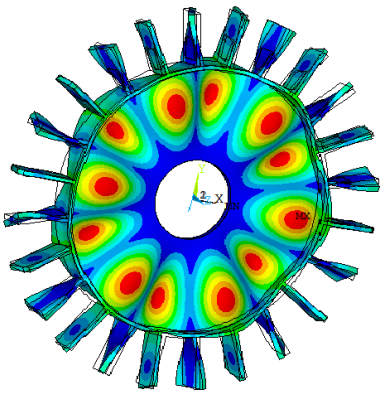

FIGURE 26. Modal shape for the blisk with SSD at short circuit state: mode (NDI 6, 4th modal group).

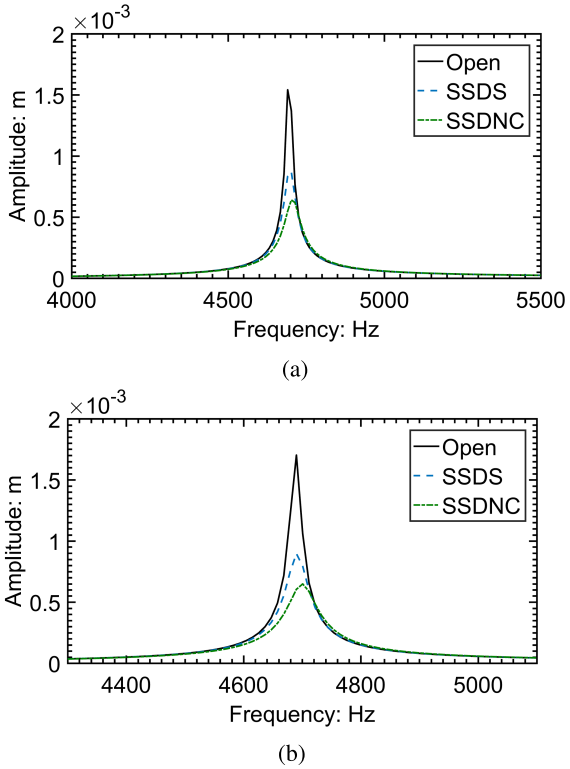

FIGURE 27. The comparison of FRFs of the blisk embedded with PZT patches at open circuit state, shunted by SSDS and SSDNC: a. for mode (NDI 8, 4th modal group); b. for mode (NDI 6, 4th modal group).

with the open circuit state, the response amplitude for SSDS and SSDNC dropped by 59% and 73%, respectively. Since the piezoelectric plate is installed at the position where the strain is large for the mode, the damping effect is good. The negative capacitance is 60% of the capacitance of the piezoelectric patch for the SSDNC shunting circuit. The damping generated by SSDNC is better than SSDS, which conforms to the theoretical basis of SSD, and similar results have been found in previous studies by using nonlinear simulations on a lumped parameter model [18]. In addition, the simulation result by linearisation is varified by HBM for the blisk with SSDNC. The simulation time is 6.21s for linearisation and 89.73s for HBM, and the relative error is less than 2% (shown in Table. 8), which demonstrates the high accuracy and efficiency of the linearisation method.

For the higher order mode dominated by blades (NDI 8, 4th modal group) and the coupling mode (NDI 6, 4th modal group) shown by Fig. 25 and 26. Blades vibrate with respect to the torsional blade mode for mode (NDI 6, 4th modal group). Fig. 27a and 27b perform the corresponding FRFs, the results of which are consistent to the previous case. Table 7 summarizes the simulation results for the aforementioned 3 modes. It is noteworthy that the same parameters are selected for piezoelectric circuits for these mode. Therefore, the damping effect of SSD is insensitive to electrical parameters. In addition, the multi-mode damping effect of SSD is also verified as shown by Fig. 28, the engine order of the excitation force is set to 6, the resonant peaks for mode (NDI 6, 1st group) and for mode (NDI 6, 4th group) both decrease significantly with SSD.

We can conclude that the proposed linearisation method can capture all the characteristics of SSD including good damping effect and multi-mode vibration reduction based

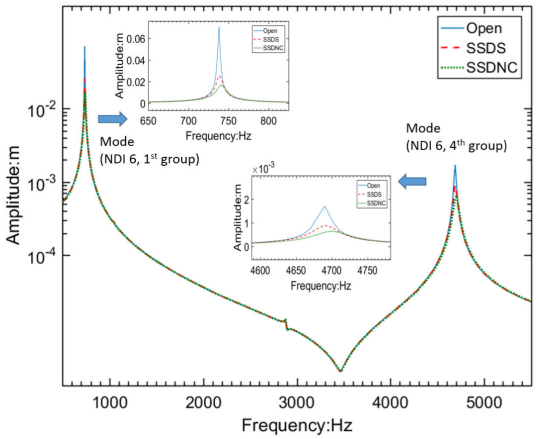

FIGURE 28. Multi-mode damping effect of SSD for modes with NDI=6.

TABLE 8. Comparison of simulation time between harmonic balance method and linearisation method for blisk model with SSDNC (NDI 6, 1st group).

Model information: blisk	DOFs per sector 5968	DOFs after reduction 463
Methods	HBM	Linearisation
Total time cost	89.73s	6.21s
Time per frequency	3.10s	0.04s
Relative Error	0%	<2%

on a dummy bllisk FE model efficiently and accurately. These findings are consistent to the results by previous studies conducted on lumped parameter models of blisks with SSD by using nonlinear solvers.

VI. CONCLUSION

This study addresses improvement of the numerical simulation efficiency for complex nonlinear systems with SSD. Considering the quasi-linear behavior of SSD systems, we have proposed and verified a linearisation method for efficient numerical simulation of complex structures with SSD.

The SSD can be simply modelled by a frequency-dependent viscous damping and a linear stiffness. These equivalent parameters are in closed-form and can be derived by the idea of equivalent dissipated energy. In addition, the lineaisation can be applied to almost every subtype of SSD (SSDS, SSDI, SSDV, SSDNC) for lumped parameter models and FE models.

The linearisation method has high computational efficiency. Compared with MHBM, the time cost of the proposed method is only 5% for the FE model of the experimental beam with SSDI and 6% for the blisk FE model with SSDNC.

The proposed method is accurate. Good agreements can be found through numerical simulation. The average relative error is about 2% compared with MHBM for steady-state analyses. Concerning the transient response under random excitation, the relative error is less than 3% compared with Newmark integral. The accuracy of the linearisation method is also verified by the published experimental data, the relative error of steady-state response of the cantilever beam with SSDI is only about 12%.

This method is especially suitable for complex structures. In this paper, the proposed method is applied to a dummy blisk with SSDNC, which is a promising application in aeronautic industry. The blisk contains more than 120k DOFs, whereas the time for calculating a frequency response curve is only 6 seconds. The vibration amplitude of the target mode is reduced by about 73%, and the multi-mode vibration reduction is achieved.

APPENDIX

The stiffness matrix of the PZT material at short circuit state $\mathbf{c}^{\mathrm{E}}$ used in the simulation reads:

$$\mathbf{c}^{\mathrm{E}}=\begin{bmatrix} C_{11}^{\mathrm{E}} & C_{12}^{\mathrm{E}} & C_{13}^{\mathrm{E}} & & & \\ C_{12}^{\mathrm{E}} & C_{11}^{\mathrm{E}} & C_{13}^{\mathrm{E}} & & & \\ C_{13}^{\mathrm{E}} & C_{13}^{\mathrm{E}} & C_{33}^{\mathrm{E}} & & & \\ & & & C_{66}^{\mathrm{E}} & & \\ & & & & C_{44}^{\mathrm{E}} & \\ & & & & & C_{44}^{\mathrm{E}} \end{bmatrix} \mathrm{Pa} \quad (37)$$

where

$$\begin{aligned} C_{11}^{\mathrm{E}} &= 13.2\times10^{10}, \quad C_{12}^{\mathrm{E}} = 5.9\times10^{10}, \; C_{13}^{\mathrm{E}} = 5.9\times10^{10} \\ C_{33}^{\mathrm{E}} &= 11.5\times10^{10}, \quad C_{44}^{\mathrm{E}} = 2.6\times10^{10}, \; C_{66}^{\mathrm{E}} = 3.0\times10^{10} \end{aligned} \quad (38)$$

The piezoelectric coupling matrix $\mathbf{e}$ reads:

$$\mathbf{e}=\begin{bmatrix} & & e_{31} \\ & & e_{31} \\ & & e_{33} \\ & e_{15} & \\ e_{15} & & \end{bmatrix} \mathrm{N/(V\cdot m)} \quad (39)$$

where

$$e_{31}=-11.6, \quad e_{33}=14.1, \quad e_{15}=10.5 \quad (40)$$

The dielectric matrix at constant strain condition ε^{s} reads:

$$\varepsilon^{s}=\varepsilon_0\begin{bmatrix} k_{11}^{\mathrm{s}} & & \\ & k_{11}^{\mathrm{s}} & \\ & & k_{33}^{\mathrm{s}} \end{bmatrix} \quad (41)$$

where

$$\varepsilon_0=8.85\times10^{12}\,\mathrm{C/(V\cdot m)}, \; k_{11}^{\mathrm{s}}=804.6, \; k_{33}^{\mathrm{s}}=659.7 \quad (42)$$

The constitutive equations of PZT materials is:

$$\begin{aligned} \mathbf{T} &= \mathbf{c}^{\mathrm{E}}\mathbf{S}-\mathbf{e}\mathbf{E} \\ \mathbf{D} &= \mathbf{e}^{\mathrm{T}}\mathbf{S}+\varepsilon^{\mathrm{s}}\mathbf{E} \end{aligned} \quad (43)$$

where $\mathbf{T}$ is mechanical stress matrix, $\mathbf{S}$ refers to mechanical strain matrix, $\mathbf{E}$ denotes electric field intensity vector and $\mathbf{D}$ refers to electric displacement vector.

ACKNOWLEDGMENT

The authors would like to acknowledge the financial support of National Natural Science Foundation of China (grant nos. 11702011 and 51675022).

REFERENCES

[1] C. Richard, D. Guyomar, D. Audigier, and G. Ching, "Semi-passive damping using continuous switching of a piezoelectric device," *Proc. SPIE*, vol. 3672, pp. 104–111, Jun. 1999.
[2] C. Richard, D. Guyomar, D. Audigier, and H. Bassaler, "Enhanced semi-passive damping using continuous switching of a piezoelectric device on an inductor," *Proc. SPIE*, vol. 3989, pp. 288–299, Apr. 2000.
[3] J. Qiu, H. Ji, and K. Zhu, "Semi-active vibration control using piezoelectric actuators in smart structures," *Frontiers Mech. Eng. China*, vol. 4, no. 3, pp. 242–251, Sep. 2009.
[4] N. W. Hagood and A. von Flotow, "Damping of structural vibrations with piezoelectric materials and passive electrical networks," *J. Sound Vibrat.*, vol. 146, no. 2, pp. 243–268, Apr. 1991.
[5] O. Thomas, J. Ducarne, and J.-F. Deü, "Performance of piezoelectric shunts for vibration reduction," *Smart Mater. Struct.*, vol. 21, no. 1, 2012, Art. no. 015008.
[6] G. Caruso, "A critical analysis of electric shunt circuits employed in piezoelectric passive vibration damping," *Smart Mater. Struct.*, vol. 10, no. 5, pp. 1059–1068, 2001.
[7] J. J. Hollkamp, "Multimodal passive vibration suppression with piezoelectric materials and resonant shunts," *J. Intell. Mater. Syst. Struct.*, vol. 5, no. 1, pp. 49–57, 1994.
[8] F. Dell'Isola, C. Maurini, and M. Porfiri, "Passive damping of beam vibrations through distributed electric networks and piezoelectric transducers: Prototype design and experimental validation," *Smart Mater. Struct.*, vol. 13, no. 2, pp. 299–308, 2004.
[9] A. Preumont, "Mechatronics: Dynamics of electromechanical and piezoelectric systems," in *Mechatronics: Dynamics of Electromechanical and Piezoelectric Systems*, vol. 136. Dordrecht, The Netherlands: Springer, 2006.
[10] E. M. Qureshi, X. Shen, and J. Chen, "Vibration control laws via shunted piezoelectric transducers: A review," *Int. J. Aeronaut. Space Sci.*, vol. 15, no. 1, pp. 1–19, 2014.
[11] A. Badel, G. Sebald, D. Guyomar, M. Lallart, E. Lefeuvre, C. Richard, and J. Qiu, "Piezoelectric vibration control by synchronized switching on adaptive voltage sources: Towards wideband semi-active damping," *J. Acoust. Soc. Amer.*, vol. 119, no. 5, pp. 2815–2825, 2006.
[12] M. Neubauer, X. Han, and J. Wallaschek, "On the maximum damping performance of piezoelectric switching techniques," *J. Intell. Mater. Syst. Struct.*, vol. 24, pp. 717–728, Apr. 2013.
[13] E. Lefeuvre, A. Badel, L. Petit, C. Richard, and D. Guyomar, "Semi-passive piezoelectric structural damping by synchronized switching on voltage sources," *J. Intell. Mater. Syst. Struct.*, vol. 17, pp. 653–660, Sep. 2006.
[14] H. Ji, J. Cheng, D. Inman, and J. Qiu, "Application of a negative capacitance circuit in synchronized switch damping techniques for vibration suppression," in *Proc. Active Passive Smart Struct. Integr. Syst.*, vol. 7643, Apr. 2010, Art. no. 76432V.
[15] H. Ji, J. Qiu, J. Cheng, and D. Inman, "Application of a negative capacitance circuit in synchronized switch damping techniques for vibration suppression," *J. Vibrat. Acoust.*, vol. 133, no. 4, 2011, Art. no. 041015.
[16] H. Ji, J. Qiu, K. Zhu, and A. Badel, "Two-mode vibration control of a beam using nonlinear synchronized switching damping based on the maximization of converted energy," *J. Sound Vibrat.*, vol. 329, no. 14, pp. 2751–2767, Jul. 2010.
[17] M. Neubauer, X. Han, and S. M. Schwarzendahl, "Enhanced switching law for synchronized switch damping on inductor with bimodal excitation," *J. Sound Vibrat.*, vol. 330, no. 12, pp. 2707–2720, 2011.
[18] J. Liu, L. Li, X. Huang, and L. Jezequel, "Dynamic characteristics of the blisk with synchronized switch damping based on negative capacitor," *Mech. Syst. Signal Process.*, vol. 95, pp. 425–445, Oct. 2017.
[19] J. Liu, L. Li, Y. Fan, and X. Huang, "A modified nonlinear modal synthesis scheme for mistuned blisks with synchronized switch damping," *Int. J. Aerosp. Eng.*, vol. 2018, Jul. 2018, Art. no. 8517890.
[20] T. M. Cameron and J. H. Griffin, "An alternating frequency/time domain method for calculating the steady-state response of nonlinear dynamic systems," *J. Appl. Mech.*, vol. 56, no. 1, pp. 149–154, Mar. 1989.
[21] C. Joannin, B. Chouvion, F. Thouverez, J.-P. Ousty, and M. Mbaye, "A nonlinear component mode synthesis method for the computation of steady-state vibrations in non-conservative systems," *Mech. Syst. Signal Process.*, vol. 83, pp. 75–92, Jan. 2017.
[22] D. Laxalde and F. Thouverez, "Complex non-linear modal analysis for mechanical systems: Application to turbomachinery bladings with friction interfaces," *J. Sound Vibrat.*, vol. 322, nos. 4–5, pp. 1009–1025, 2009.
[23] J. Liu, L. Li, and Y. Fan, "A comparison between the friction and piezoelectric synchronized switch dampers for blisks," *J. Intell. Mater. Syst. Struct.*, vol. 29, no. 12, pp. 2693–2705, 2018.
[24] Y. Wu, Y. Fan, L. Li, and J. Liu, "Sensitivity analysis and design of an open-loop active normal force for dry friction dampers," in *Proc. Conf. Smart Mater., Adapt. Struct. Intell. Syst.*, Sep. 2017, Art. no. V002T03A006.
[25] J. M. Borrajo, S. Zucca, and M. M. Gola, "Analytical formulation of the jacobian matrix for non-linear calculation of the forced response of turbine blade assemblies with wedge friction dampers," *Int. J. Non-Linear Mech.*, vol. 41, no. 10, pp. 1118–1127, Dec. 2006.
[26] R. M. Rosenberg, "The normal modes of nonlinear n-degree-of-freedom systems," *J. Appl. Mech.*, vol. 29, no. 1, pp. 7–14, 1962.
[27] X.-R. Huang, L. Jézéquel, S. Besset, L. Li, and O. Sauvage, "Nonlinear modal synthesis for analyzing structures with a frictional interface using a generalized masing model," *J. Sound Vibrat.*, vol. 434, pp. 166–191, Nov. 2018.
[28] W. Szemplińska-Stupnicka, "The modified single mode method in the investigations of the resonant vibrations of non-linear systems," *J. Sound Vibrat.*, vol. 63, no. 4, pp. 475–489, Apr. 1979.
[29] Y. G. Wu, L. Li, Y. Fan, H. Y. Ma, W. J. Wang, J.-L. Christen, and M. Ichchou, "Design of semi-active dry friction dampers for steady-state vibration: Sensitivity analysis and experimental studies," *J. Sound Vibrat.*, vol. 459, Oct. 2019, Art. no. 114850.
[30] G. Kerschen, M. Peeters, J. C. Golinval, and A. F. Vakakis, "Nonlinear normal modes, Part I: A useful framework for the structural dynamicist," *Mech. Syst. Signal Process.*, vol. 23, no. 1, pp. 170–194, 2009.
[31] J.-F. Shi, Y.-L. Zhang, and X.-F. Gou, "Bifurcation and evolution of a forced and damped duffing system in two-parameter plane," *Nonlinear Dyn.*, vol. 93, no. 2, pp. 749–766, Jul. 2018.
[32] M. Krack, "Nonlinear modal analysis of nonconservative systems: Extension of the periodic motion concept," *Comput. Struct.*, vol. 154, pp. 59–71, Jul. 2015.
[33] H. Ji, J. Qiu, K. Zhu, Y. Chen, and A. Badel, "Multi-modal vibration control using a synchronized switch based on a displacement switching threshold," *Smart Mater. Struct.*, vol. 18, no. 3, 2009, Art. no. 035016.
[34] J. H. Griffin, "A review of friction damping of turbine blade vibration," *Int. J. Turbo Jet Engines*, vol. 7, nos. 3–4, pp. 297–308, Dec. 1990.
[35] C. M. Firrone and S. Zucca, "Modelling friction contacts in structural dynamics and its application to turbine bladed disks," in *Numerical Analysis—Theory and Application*, J. Awrejcewicz, Ed. Rijeka, Croatia: InTech, Sep. 2011, pp. 301–334.
[36] D. Laxalde, F. Thouverez, and J.-P. Lombard, "Forced response analysis of integrally bladed disks with friction ring dampers," *J. Vibrat. Acoust.*, vol. 132, no. 1, 2010, Art. no. 011013.
[37] J. Tang and K. W. Wang, "Vibration control of rotationally periodic structures using passive piezoelectric shunt networks and active compensation," *J. Vibrat. Acoust.*, vol. 121, no. 3, pp. 379–390, 1999.
[38] B. Zhou, F. Thouverez, and D. Lenoir, "An adaptive control strategy based on passive piezoelectric shunt techniques applied to mistuned bladed disks," *J. Comput. Appl. Math.*, vol. 246, pp. 289–300, Jul. 2013.
[39] L. Li, P. Deng, and Y. Fan, "Dynamic characteristics of a cyclic-periodic structure with a piezoelectric network," *Chin. J. Aeronaut.*, vol. 28, no. 5, pp. 1426–1437, Oct. 2015.

YAGUANG WU was born in Beijing, China, in 1990. He received the B.S. degree in applied mathematics and the M.S. degree in power engineering from Beihang University, China, in 2013 and 2016, respectively, and the Engineer degree from Centrale Nantes, France, in 2016. He is currently pursuing the Ph.D. degree in aerospace engineering with Beihang University.

His research interests include design methodology of dry friction/piezoelectric hybrid damper and the implementation of piezoelectric damping technologies in aerospace domain.

LIN LI was born in Hebei, China, in 1956. She received the Ph.D. degree from Pierre and Marie Curie University, France, in 1988.

She has been a Professor with Beihang University, since 1996. She is the Principle Investigator of more than 30 research projects funded by aerospace industries, shipbuilding companies, and National Natural Science of China. She coauthored more than 100 publications, in which more than 30 of them are international journal and conference papers. Her current research interests include the vibration suppression of turbomachinery under fluid excitation, dynamic analysis, and the vibration control of smart materials and structures.

YU FAN was born in Sichuan, China, in 1987. He received the Ph.D. degree from the Ecole Centrale de Lyon, France, in 2016. He is currently with Beihang University as an Associate Professor.

He has been the Council Member of the Chinese Society for Vibration Engineering (CSVE), since 2018. He has been an Associate Professor with Beihang University, since 2019. He has coauthored more than 20 international publications, 10 national publications, and 2 books, and holds 5 patents. He is the Principle Investigator of five national research projects and is involved in several industrial research projects. His current research interests include piezoelectric structures, wave propagation, and vibration control.

He received the Seal of Excellence of Horizon 2020's Marie Sklodowska-Curie actions, in 2019.

JIUZHOU LIU was born in Jilin, China, in 1988. He received the B.S. and Ph.D. degrees in aerospace engineering from Beihang University, Beijing, China, in 2012 and 2018, respectively.

Since 2018, he has been a Senior Engineer with the China Academy of Launch Vehicle Technology, Beijing. His research interests include dry friction damper design and piezoelectric damping technologies.

QIAN GAO was born in Jiangsu, China, in 1995. He received the B.S. degree in aircraft engineering from the Nanjing University of Aeronautics and Astronautics, Jiangsu, China, in 2018. He is currently pursuing the Ph.D. candidate in aerospace engineering with Beihang University, China.